

Resonance Raman Characterization of Excitonically Coupled *meso,meso*-Linked Porphyrin Arrays[†]

Anwar A. Bhuiyan,[‡] Jyoti Seth,[‡] Naoya Yoshida,[§] Atsuhiko Osuka,[§] and David F. Bocian^{*,‡}

Department of Chemistry, University of California, Riverside, California 92521-0403, and Department of Chemistry, Graduate School of Science, Kyoto University, Kyoto 606-8502, Japan

Received: January 25, 2000; In Final Form: May 1, 2000

Resonance Raman (RR) spectra are reported for dimeric, trimeric, and tetrameric porphyrin arrays in which the porphyrins are directly linked at the *meso* position. The RR spectra of two monomeric building blocks of the arrays are also examined. The close proximity and orthogonal orientation of adjacent porphyrins in the arrays result in exceptionally strong excitonic interactions along the axis defined by the *meso,meso*-linkage(s) and negligible interactions along the orthogonal axis. The coupling scheme breaks the degeneracy of the B excited state and leads to two B(0,0) absorption features. One feature, designated B_x(0,0), is the supermolecule absorption that is strongly red-shifted, due to exciton coupling. The other feature, designated B_y(0,0), is the superposition of absorptions of the orthogonal, individual porphyrins. This latter absorption occurs at approximately the same energy as the B(0,0) band of a monomeric porphyrin, due to the absence of excitonic interactions. The exciton coupling in the Q state is much weaker than that in the B state, due to the smaller oscillator strength of the former transition. The B-state excitation RR spectra of the *meso,meso*-linked arrays exhibit a complex and unusual scattering pattern. The most striking features are (1) the appearance of only polarized and anomalously polarized modes in the RR spectrum, (2) the intensity enhancement of anomalously polarized vibrations with B-state excitation, and (3) the large differential enhancement of symmetric versus nontotally symmetric vibrations with excitation across the B-state absorptions. All of these scattering characteristics are due to the effects of symmetry lowering. The asymmetric *meso* substitution pattern inherent to the *meso,meso*-linked arrays contributes to symmetry lowering in both the ground and excited electronic states. The strong uniaxial excitonic interactions make an additional contribution to symmetry lowering in the excited state(s). This latter characteristic promotes novel Franck–Condon and vibronic scattering mechanisms in the B state(s) of the arrays. Collectively, the studies of the *meso,meso*-linked arrays provide insight into the type of RR scattering that might be anticipated for other types of systems that exhibit strong excitonic interactions among the constituents.

Introduction

Natural photosynthetic systems employ elaborate light-harvesting complexes to capture dilute sunlight and funnel the captured energy to the reaction center through rapid and efficient transfer processes.¹ The light-harvesting complexes in the natural system are generally composed of electronically coupled chlorophyll (or bacteriochlorophyll) molecules assembled in protein matrixes that absorb over a wide spectral range. The challenge of creating artificial mimics of the light-harvesting complexes has led to the design and synthesis of a diverse collection of multiporphyrin arrays. Examples of covalently linked architectures comprised of five or more porphyrins include the following: (1) dendritic arrays with stilbene linkers,² diphenylethyne linkers,³ or a combination of diphenylethyne and ester linkers,⁴ (2) windmill arrays with direct *meso,meso*-linkages,⁵ (3) sheetlike arrays with Pd-coordinated pyridyl linkages,⁶ (4) star-shaped arrays with diphenylethyne linkers,^{7,8} oligophenylethyne linkers,⁹ phenylene linkers,^{10,11} phenylenevinylene linkers,¹² or benzoxypheyl linkers,¹³ (5) linear arrays

with phenylene linkers¹⁴ or 1,3,5-triazine units joining aniline groups,¹⁵ (6) cyclic arrays with diphenylbutadiene linkers¹⁶ or diphenylethyne linkers,¹⁷ and (7) backbone polymeric arrays with oligophenylenevinylene linkers^{18,19} or phenylethyne linkers.²⁰ The extent of electronic interaction between the porphyrin constituents in these different classes of arrays varies considerably, depending on both the length and type of linker (the latter of which controls the relative orientation of the porphyrins). The largest electronic interactions are observed in architectures that contain direct *meso,meso*-linked porphyrins. The close proximity of the porphyrins in these assemblies results in excitonic interactions that are several tenths of an electronvolt.²¹

Resonance Raman (RR) spectroscopy is a particularly sensitive probe of the structural and electronic properties of metalloporphyrin complexes. Metalloporphyrins produce extremely intense and detailed RR spectra that have been interpreted successfully by using models for vibronically induced scattering from the porphyrin B (Soret) and Q states.²² RR techniques were used early on in attempts to characterize interporphyrin interactions in a variety of covalently linked dimeric assemblies, including the following: (1) axially bridged iron complexes (TPPFe)₂X, where (TPP = tetraphenylporphyrin, X = O,^{23,24} N,²⁵ C²⁶), (OEPFe)₂X, where (OEP = octaethylporphyrin, X =

[†] Part of the special issue "Thomas Spiro Festschrift". Dedicated to Thomas G. Spiro on the occasion of his 65th birthday.

[‡] University of California.

[§] Kyoto University.

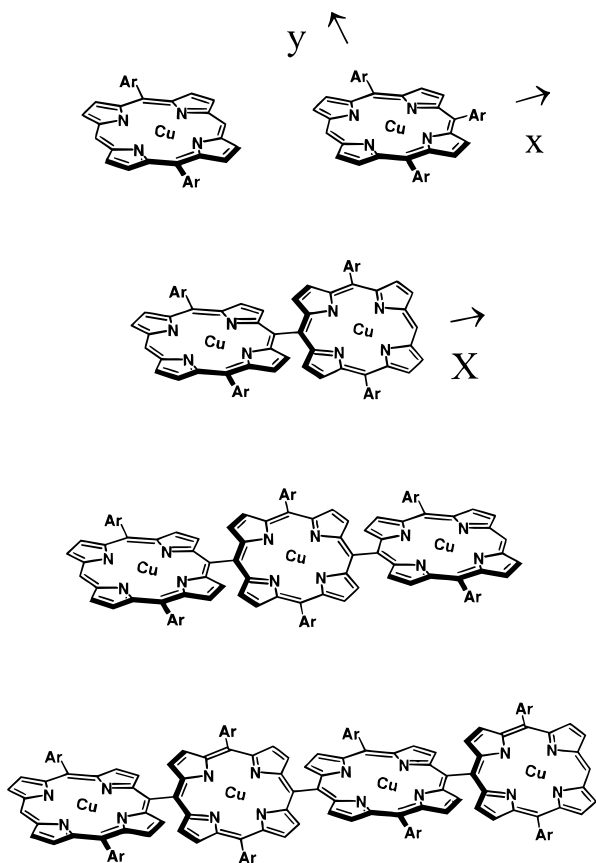


Figure 1. Structures of the *meso,meso*-linked porphyrin arrays.

O, N),²⁷ and (OECFe)₂O,²⁸ where (OEC = octaethylchlorin); (2) lanthanide sandwich complexes (TPP)₂Ln, where (Ln = Ce, La),^{29a,b} (OEP)₂Ln, where (Ln = Ce, La, Eu, Nd),^{29b} and (TPP)-(OEP)Ce;^{29c} and (3) transition metal–metal-bonded complexes (OEMP)₂, where (M = Os, Re, Mo).³⁰ The common structural feature shared by all of these dimers is that the porphyrin rings are face-to-face. The electronic coupling between the porphyrins ranges from quite strong in the lanthanide sandwich dimers to relatively weak in the axially bridged iron and transition metal–metal-bonded dimers. Interestingly, even the most strongly electronically coupled dimers do not exhibit any evidence for intradimer vibrational coupling in the ground electronic state.²⁹ The same is also the case for the extended strongly coupled face-to-face assembly, the (OEP)₃Eu₂ triple decker.³¹ More recently, RR techniques have been used to investigate other types of covalently linked assemblies, including star-shaped arrays,^{7,8b,c} a molecular square,³² and their dimeric and trimeric (both linear and right-angle) building blocks.³³ All of these latter arrays are joined via diarylethylene linkers, and the interporphyrin electronic communication is relatively weak. As a consequence, the vibrational spectra of these arrays resemble those of the isolated constituent porphyrins.

At this time, the only strongly (electronically) coupled porphyrinic assembly that has been subjected to detailed vibrational scrutiny is (OEP)₃Eu₂. To further investigate the structural and electronic properties of strongly coupled multiporphyrin arrays, we have examined the RR scattering characteristics of the dimeric, trimeric, and tetrameric *meso,meso*-linked assemblies shown in Figure 1. Both the diaryl- and triaryl-substituted (aryl = 3,5-di-*tert*-butylphenyl) monomeric building blocks were also examined. The studies of the *meso,meso*-linked arrays reveal novel RR scattering characteristics that have not been previously observed for metalloporphyrins.

Experimental Section

Sample Preparation. The various porphyrin complexes were prepared as previously described.²¹ The porphyrins were initially prepared as Zn(II) complexes. Zinc was removed from the complexes by treatment with aqueous HCl. Cu(II) was inserted into the complexes using the standard procedure with Cu(OAc)₂.³⁴ To a solution of free base porphyrin (20–100 mg) in CH₂Cl₂ (50–200 mL) was added a saturated solution of Cu(OAc)₂ in methanol (1–3 mL). The resulting solution was refluxed for 2 h. After the usual workup, the Cu(II) complexes were purified by silica gel chromatography and recrystallized from CH₂Cl₂ and methanol. The molecular weights were measured by the MALDI-TOF MS method. Monomer *m/e* = 747, calcd for C₄₈H₅₂N₄Cu = 747.3; dimer *m/e* = 1495, calcd for C₉₆H₁₀₂N₈Cu₂ = 1493; trimer *m/e* = 2242, calcd for C₁₄₄H₁₅₂N₁₂Cu₃ = 2241; tetramer *m/e* = 2988, calcd for C₁₉₂H₂₀₂N₁₆Cu₄ = 2987.

Absorption Spectra. The absorption spectra of the porphyrin complexes were obtained with a Hewlett-Packard Model 8452A diode array spectrometer. The spectra were obtained in the 300–800 nm range in the absorbance mode. All spectra were obtained at room temperature in CH₂Cl₂ solutions; the sample concentration was typically ~0.01 mM.

RR Spectra. The RR spectra of the complexes were obtained with a triple spectrograph (Spex 1877) equipped with either a 1800 groove/mm (Q-excitation) or 2400 groove/mm (B-excitation) holographically etched grating in the final stage. A liquid nitrogen cooled, UV-enhanced 1152 × 298 pixel charge-coupled device (Princeton Instruments, LN/CCD equipped with an EEV 1152-UV chip) was used as the detector. The excitation wavelengths were obtained from a Kr ion laser (Coherent Innova 200-K3), an Ar ion laser (Coherent Innova 400-15UV), and a dye laser (Coherent CR 590) using Stilbene 3 (Lamda Physik, Inc.) pumped by the multiline UV output of an Ar ion laser (Coherent Innova 400-15UV). All spectra were obtained at room temperature in CH₂Cl₂ solutions; the sample concentrations were in the 0.05–0.5 mM range. To mitigate photodecomposition, the sample was placed in a rotating NMR tube. The NMR tube was illuminated by a laser beam focused through a lens, and the scattering was collected at an angle 90° to the incident laser beam by using a camera lens (Canon 50 mm) collection system. The laser power at the sample was typically in the 10–20 mW range. Absorption spectra of the samples obtained before and after the RR measurements were found to be identical, indicating that no significant photodecomposition occurred during the course of the RR experiments. The spectra were calibrated by using the known frequencies of indene and are accurate to ±2 cm⁻¹. The relative intensities for the polarization measurements were obtained from the peak heights in the recorded spectra using the 1423 cm⁻¹ band of CH₂Cl₂ as the internal standard.

IR Spectra. The IR spectra were measured on a Bruker Equinox 55 Fourier transform IR spectrophotometer. The spectra were obtained at room temperature on polyethylene film IR cards in the region 900–1600 cm⁻¹. The complexes were dissolved in CH₂Cl₂, and the concentrated solutions were spread on the film. The solvent was evaporated by blowing air over the film. The film was then placed in the sample compartment of the spectrophotometer and purged with dry air for 5 min. A polyethylene film IR card from which neat CH₂Cl₂ had been evaporated was used as the background. The reproducibility of the spectra was checked by multiple scans.

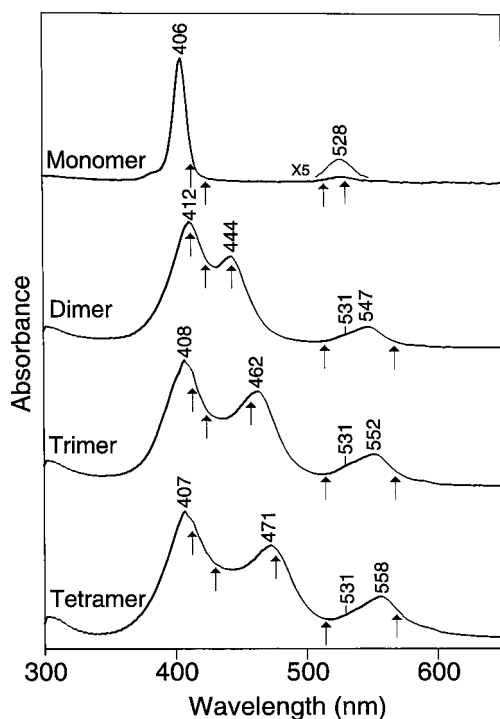


Figure 2. Absorption spectra (295 K) of the *meso,meso*-linked porphyrin arrays in CH_2Cl_2 . The arrows indicate the excitation wavelengths used in the RR studies.

Results and Discussion

Absorption Spectra. The absorption spectra of the diaryl-substituted monomer and the three *meso,meso*-linked arrays are shown in Figure 2. The spectrum of the triaryl-substituted monomer (not shown) is similar to that of the diaryl-substituted monomer. The spectra of both monomers are also similar to that of CuTPP (not shown).³⁵ However, the number of aryl substituents does affect the positions of the band maxima (diaryl-substituted monomer, $B(0,0) = 406$ nm, $Q(1,0) = 528$ nm; triaryl-substituted monomer, $B(0,0) = 412$ nm, $Q(1,0) = 534$ nm; CuTPP, $B(0,0) = 416$ nm, $Q(1,0) = 539$ nm). The optical spectra of the Cu(II) complexes of the *meso,meso*-linked porphyrins investigated here exhibit the same general characteristics as previously reported for the Zn(II) analogues.²¹ In particular, all three *meso,meso*-linked arrays exhibit two $B(0,0)$ bands. The maximum of one $B(0,0)$ band of each array occurs at approximately the same wavelength as the $B(0,0)$ band of the monomeric *meso*-aryl-substituted porphyrins (406–416 nm). The maximum of the other $B(0,0)$ band is appreciably red-shifted and moves systematically to lower energy as the size of the array increases (dimer, 444 nm; trimer, 462 nm; tetramer, 471 nm). The behavior of the $Q(1,0)$ bands of the *meso,meso*-linked arrays is qualitatively similar to that of the $B(0,0)$ bands. For the $Q(1,0)$ bands, a shoulder is observed at approximately 531 nm for each array, which is in the same wavelength regime as the $Q(1,0)$ bands of monomeric *meso*-aryl-substituted porphyrins (528–537 nm). The second $Q(1,0)$ band of the arrays is red-shifted (dimer, 547 nm; trimer, 552 nm; tetramer, 558 nm), but to a much lesser extent than the analogous $B(0,0)$ band. The extent of the red-shift of the second $Q(1,0)$ band of the arrays as a function of array size appears to be less systematic than that of the second $B(0,0)$ band. However, the $Q(1,0)$ bands are quite broad and much weaker, which precludes an accurate identification of the band maximum.

The trends observed in the optical spectra of the *meso,meso*-linked arrays are consistent with excitonic interactions between

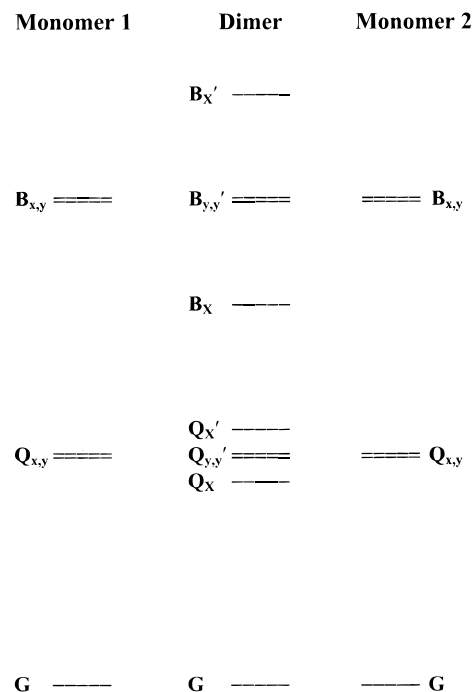


Figure 3. Schematic energy level diagram for the *meso,meso*-linked dimer. The transitions to the excitonic states B_x and Q_x are allowed, whereas those to the excitonic states $B_{x'}$ and $Q_{x'}$ are forbidden (see text). The transitions to the monomer-like states $B_{y,y'}$ and $Q_{y,y'}$ are allowed. The energy splittings shown in the diagram are not to scale.

the porphyrins, as has been previously discussed.²¹ A coupling scheme that accounts for the spectral features is as follows: the transitions to the Q- and B-excited states of metalloporphyrins are in-plane (x, y) and (approximately) degenerate (E_u in D_{4h} symmetry).³⁵ Thus, the choice of axes for the electronic transitions is arbitrary (see Figure 1). If the lines through opposite methine carbons are chosen as the axes, one axis of the array (X) is along the *meso,meso*-linkage(s). Strong excitonic interactions are expected along this axis because the transition dipoles of the individual porphyrins are in-line (note that the dipole-dipole interactions along this axis are independent of the torsional angle between adjacent porphyrins).³⁶ On the other hand, the close proximity of the porphyrins in the arrays dictates that the planes of adjacent rings and, accordingly, the y -axes of nearest neighbor porphyrins are (nearly) orthogonal (due to steric constraints). The dipolar exciton coupling in the orthogonal orientation vanishes.³⁶ This feature obviates the utility of defining a Y -axis for the arrays. It should also be noted that the excitonic interactions between non-nearest neighbor, coplanar porphyrins in the trimer and tetramer are expected to be negligible, owing to the substantial distance between these constituents. The orthogonal orientation of adjacent porphyrins in the arrays also precludes any conjugation between these constituents. This situation can be contrasted with that of porphyrin arrays with linkers such as butadiyne wherein strong conjugative effects are observed.³⁷

The strong excitonic interactions between the in-line transition dipoles along the X -axis of the arrays combined with the null interactions between the transition dipoles along the y -axes of the constituents formally break the degeneracy of the Q- and B-excited states of the individual porphyrins in the array. A schematic energy level diagram indicating the excitonic splittings of Q- and B-excited states is shown in Figure 3. The in-line orientation of the transition dipoles along the X -axis dictates that the transition to the lowest energy excitonic state (B_x or Q_x) is strongly allowed, whereas the transition to the highest

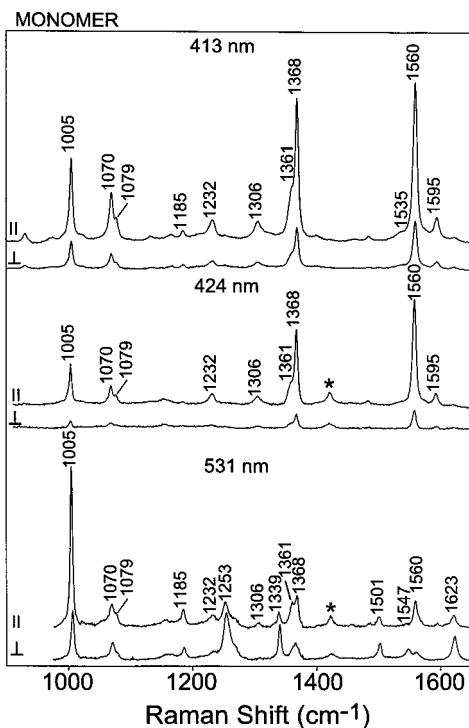


Figure 4. RR spectra of the diaryl-substituted monomer in CH_2Cl_2 . The bands marked by the asterisks are due to solvent.

energy state (B_X' or Q_X') is forbidden.³⁶ The transitions to the other excitonic states that occur at intermediate energies for the higher order aggregates (trimer and tetramer) are also only weakly allowed. The transition to the lowest energy B excitonic state, designated $B_X(0,0)$, is a supermolecular transition that gives rise to the highly red-shifted B(0,0) band of the arrays. The exciton coupling energy for the arrays can be extracted from plots of the exciton splitting, ΔE , versus $2 \cos[\pi/(N + 1)]$, where N = array size.³⁶ Previous studies of the Zn(II) complexes of the *meso,meso*-linked arrays have shown that this plot is linear with a slope of $\sim 4200 \text{ cm}^{-1}$.^{21,38} This is also the case for the Cu(II) complexes studied here. The exciton coupling energy between adjacent porphyrins in the arrays is half the value of the slope,³⁶ or $\sim 2100 \text{ cm}^{-1}$. The transition to the lowest energy Q excitonic state gives rise to the (less) red-shifted Q(1,0) band. The red shifts of the Q(1,0) bands are smaller than those of the analogous B bands, owing to the smaller transition dipole moment of the former state. This feature, combined with the breadth of the absorption band, precludes an accurate determination of the Q-state exciton coupling energy. The electronic transitions polarized along the y -axes of the individual porphyrins are energetically nearly coincident due to the general structural similarity of the porphyrins in the arrays and the absence of excitonic interactions between the orthogonal transition dipoles. This results in B(0,0) and Q(1,0) absorption features that are at approximately the same energy as a monomer. For convenience, this B-state absorption is designated $B_y(0,0)$, even though it represents multiple transitions.

Vibrational Spectra. The high-frequency regions (1000 – 1650 cm^{-1}) of the RR spectra of the diaryl-substituted monomer and the three *meso,meso*-linked arrays obtained with selected exciting lines are shown in Figures 4–7. The IR spectra of the various complexes are shown in Figure 8. The RR spectra of the triaryl-substituted monomer (not shown) are similar to those of the diaryl-substituted monomer. The spectra of both monomers are also similar to those of CuTPP (not shown).³⁹ The frequencies of most of the RR bands of the three types of

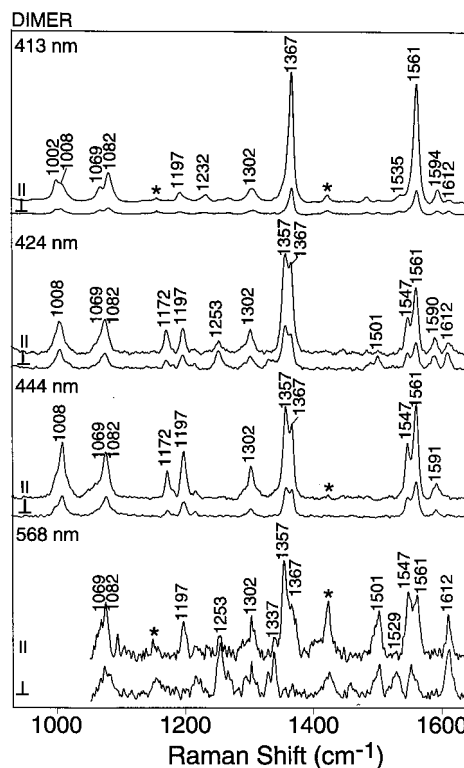


Figure 5. RR spectra of the dimer in CH_2Cl_2 . The bands marked by the asterisks are due to solvent.

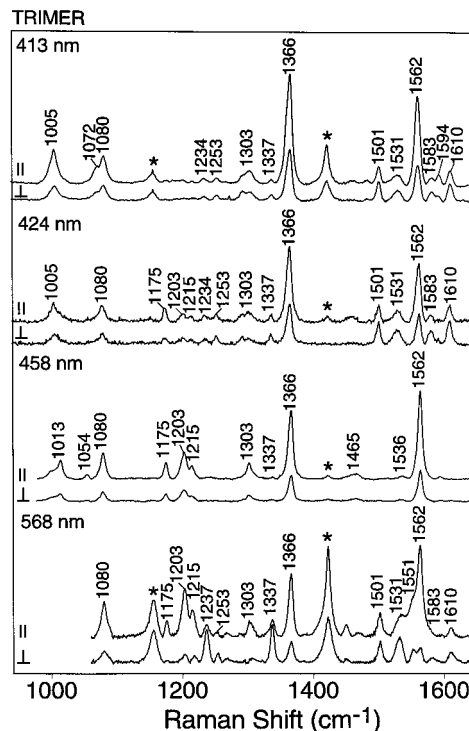


Figure 6. RR spectra of the trimer in CH_2Cl_2 . The bands marked by the asterisks are due to solvent.

monomers are very similar. Accordingly, the spectra were assigned by analogy to the assignments previously reported for CuTPP³⁹ (and NiTPP⁴⁰). The frequencies of the RR bands of all three *meso,meso*-linked arrays are also similar to those of the monomers. Accordingly, the RR bands for the arrays were also assigned by analogy. The assignments for selected RR bands attributable to porphyrin ring skeletal modes are summarized in Table 1. Detailed assignments of the IR bands are

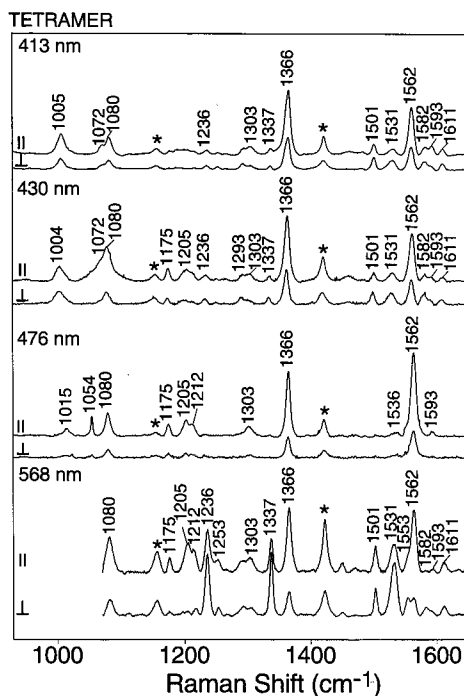


Figure 7. RR spectra of tetramer in CH_2Cl_2 . The bands marked by the asterisks are due to solvent.

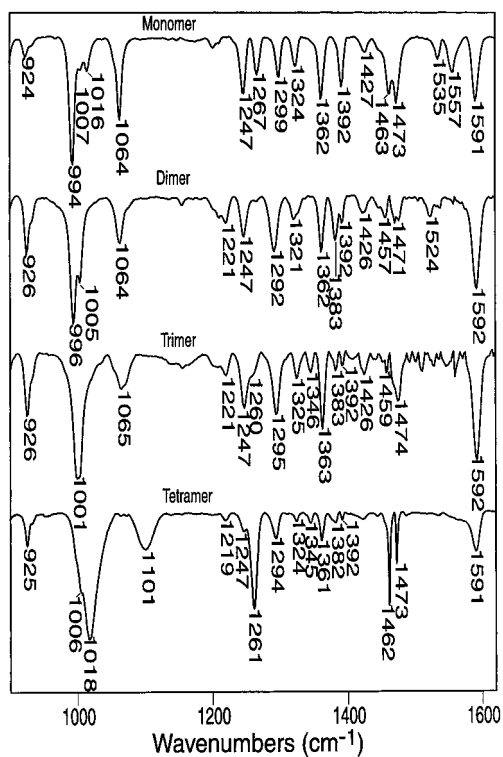


Figure 8. IR spectra of the thin films of porphyrin complexes on polyethylene.

not included in the table. These data proved less useful because comparison of the IR spectra of the various porphyrin complexes with that of the 1,3-ditertbutylbenzene (the aryl substituent of the arrays) (not shown) revealed that most of the IR features observed for the porphyrin complexes are attributable to the aryl substituents.

Although many similarities exist between the RR spectra of the *meso,meso*-linked arrays and the various monomeric porphyrins, including CuTPP, there are certain notable differences. These differences include (1) the vibrational and (2) the

polarization characteristics of certain modes of the *meso,meso*-linked arrays and the monomeric building blocks versus CuTPP and (3) the B-state RR enhancement patterns for the *meso,meso*-linked arrays versus the various monomeric *meso*-aryl-substituted porphyrins, including CuTPP. As will be discussed below, all of these scattering characteristics are due to the effects of symmetry lowering. The asymmetric *meso* substitution pattern inherent in the *meso,meso*-linked arrays (and diaryl- and triaryl-substituted monomers) contributes to symmetry lowering in both the ground and excited electronic states. The strong uniaxial excitonic interactions make an additional contribution to symmetry lowering in the excited state(s). This latter characteristic promotes novel Franck–Condon and vibronic scattering mechanisms in the B state(s) of the arrays.

Vibrational Characteristics of the meso,meso-Linked Arrays and the Monomeric Building Blocks. The *meso* substituents and substitution pattern in the diaryl- and triaryl-substituted monomers and the *meso,meso*-linked arrays differ from that of TPP (Figure 1). All of the complexes contain *meso*-3,5-di-*tert*-butyl rather than phenyl groups. At first approximation, the structural differences between these two types of *meso* substituents would not be expected to perturb the vibrational characteristics of the porphyrin rings. On the other hand, the *meso* substitution pattern in both the diaryl- and triaryl-substituted monomers and all three arrays is highly asymmetric and does alter the vibrational characteristics of the porphyrins. The asymmetry in the monomers is due to the presence of *meso* hydrogen atoms. Both porphyrins in the dimer and the two terminal porphyrins in the trimer and tetramer also have a hydrogen atom at the outer *meso* position. However, these porphyrins have a porphyrin at the other *meso* position rather than an aryl group. The central porphyrin(s) of the trimer and tetramer have two porphyrin substituents at the *meso* positions.

The asymmetric *meso* substitution pattern in the diaryl- and triaryl-substituted monomers and the constituent porphyrins in the arrays breaks the (approximate) 4-fold symmetry of the ground electronic state of the individual porphyrins. The substitution pattern formally mixes the A_{1g} and B_{2g} (RR active) vibrations and the A_{2g} and B_{1g} vibrations (RR active). The substitution pattern also formally splits the E_u modes (IR active) and mixes one member of the E_u pair with the A_{1g}/B_{2g} set and the other member of the E_u pair with the A_{2g}/B_{1g} set. These perturbations, along with mass effects (hydrogen atoms versus aryl groups or porphyrins), most appreciably affect vibrations involving atoms at the site of the perturbation, in particular, the methine bridge stretches, $\nu_{C_aC_m}$, and the porphyrin–aryl group stretches, $\nu_{C_aC_{aryl}}$. The behavior of these modes is discussed in more detail below.

The $\nu_{C_aC_m}$ vibrations of MTPP complexes include $\nu_{10}(B_{1g})$, $\nu_{19}(A_{2g})$, and $\nu_{37}(E_u)$. The ν_{10} , ν_{19} , and ν_{37} modes of CuTPP are observed at 1583, 1531, and 1574 cm^{-1} , respectively.^{36,41} Comparison of the RR spectra of the diaryl- and triaryl-substituted monomers and CuTPP shows that both ν_{10} and ν_{19} systematically upshift as the number of *meso*-aryl groups decreases (ν_{10} , 1585, 1612, and 1623 cm^{-1} ; ν_{19} , 1531, 1540, and 1547 cm^{-1}). This trend is also consistent with the vibrational characteristics reported for NiTPP versus NiP (P = porphine, which contains hydrogen atoms at all four *meso* positions). The presence of four *meso* hydrogens in NiP upshifts ν_{10} and ν_{19} even more substantially (50–60 cm^{-1} relative to those of NiTPP).⁴⁰ The vibrational studies of NiTPP and NiP indicate that ν_{37} should also follow this same trend. However, the only IR bands for the diaryl- and triaryl-substituted monomers that appear to be candidates for ν_{37} are observed at 1557 and 1565

TABLE 1: Selected RR Bands (cm⁻¹) of the Complexes Assignable to Porphyrin Skeletal Modes

monomer	dimer	trimer	tetramer	polarization ^a	assignment ^b
1623, 1612, 1585 ^c	1612	1610, 1583 ^d	1611, 1582 ^d	ap(dp) ^e	ν_{10}
1560	1561	1562	1562	p	ν_2
1557, 1565, 1574 ^{c,f}	1547	1551	1553	p	ν_{37}
1535, 1535, 1538 ^{c,g}	1535	1536	1536	p	ν_{38}
1547, 1540, 1531 ^c	1529	1531	1531	ap	ν_{19}
1501	1501 ^h	1501	1501	ap(dp) ^e	ν_{11}
1368	1367	1366	1366	p	ν_4
1361	1357			p	ν_{29}
1339	1337	1337	1337	ap	ν_{20}
1306	1302	1303	1303	p(dp) ^e	ν_{12}
1253, 1253, 1232 ^c	1253	1253, 1232 ^d	1253, 1236 ^d	ap	ν_{26}
1232	1232	1234	1236	p	ν_1
		1215	1212	p	$\nu(\text{C}_m\text{C}_m)$
	1197	1203	1205	p	$\nu(\text{C}_m\text{C}_m)$
1185	1172	1175	1175	p	ν_{34}
1079	1082	1080	1080	p(dp) ^e	ν_{17}
1070	1079	1072	1072	p	ν_{47}
1005	1008	1005	1005	p	ν_6

^a Abbreviations: p, polarized; ap, anomalously polarized; dp, depolarized. ^b Taken from refs 39–41. ^c Observed for the diaryl-substituted monomer, triaryl-substituted monomer, and CuTPP, respectively (see text). ^d These bands are assigned to the terminal and central rings, respectively (see text). ^e The polarization listed in parentheses is that observed for CuTPP and /or NiTPP (see text). ^f These frequencies are taken from the IR spectra. ^g The frequency for CuTPP was taken from the IR spectrum. ^h This band is ap at all excitation wavelengths, with the exception of 568 nm, for which the band is p (see text).

cm⁻¹, respectively (versus 1574 cm⁻¹ for CuTPP). Accordingly, the trend in frequency versus number of *meso*-aryl groups is opposite that observed for ν_{10} and ν_{19} . This reversal most likely occurs because ν_{37} splits in the lower symmetry environment of the diaryl- and triaryl-substituted complexes. The trends observed in the frequencies of the ν_{37} modes suggest that the magnitude of the splitting is largest for the diaryl-substituted monomer. The effects of symmetry lowering apparently outweigh the effects of changing the mass of the *meso* substituent.

The $\nu_{\text{C}_m\text{C}_m}$ vibrations of the *meso,meso*-linked arrays were assigned using the above-noted trends as a reference point. For example, the ν_{10} mode of the dimer is observed at 1612 cm⁻¹, a frequency identical to that observed for the analogous mode of the triaryl-substituted monomer. A ν_{10} mode of the trimer and the tetramer is also observed at \sim 1612 cm⁻¹. A second ν_{10} mode is observed for both of these arrays at \sim 1583 cm⁻¹. This latter frequency is nearly identical to that observed for the ν_{10} mode of CuTPP. Accordingly, the \sim 1612 and \sim 1583-cm⁻¹ bands of the trimer and tetramer are attributed to the ν_{10} vibrations of the terminal and central porphyrins, respectively. This same strategy was used to assign the ν_{19} and ν_{37} modes of the porphyrins in the *meso,meso*-linked arrays. Interestingly, the latter mode is not clearly visible in the IR spectra but is activated in the RR spectra (due to symmetry lowering). For both the ν_{19} and ν_{37} modes, the frequency matching with modes of the monomeric porphyrins is not as good as that for ν_{10} . In addition, for the trimer and tetramer, two distinct bands assignable to the ν_{19} and ν_{37} vibrations of the terminal and central porphyrins could not be identified. However, the RR bands due to both of these vibrations lie in very congested spectral regions and may be obscured by other stronger bands.

The $\nu_{\text{C}_m\text{C}_{\text{aryl}}}$ vibrations of MTPP complexes include $\nu_1(\text{A}_{1g})$, $\nu_{27}(\text{B}_{2g})$, and $\nu_{36}(\text{E}_u)$. Both ν_1 and ν_{27} are RR active and are observed for CuTPP at 1238 and 1269 cm⁻¹, respectively.³⁵ The ν_{36} mode is IR active but not observed.⁴⁰ The RR spectra of the diaryl- and triaryl-substituted monomers both exhibit a band similar to ν_1 at \sim 1232 cm⁻¹; a band similar to ν_{27} could not be identified. A ν_1 -like feature is also observed at \sim 1232 cm⁻¹ for all three *meso,meso*-linked arrays. A more interesting question for the arrays is whether the interporphyrin C_mC_m stretches, $\nu_{\text{C}_m\text{C}_m}$, are observed in the RR spectrum. The $\nu_{\text{C}_m\text{C}_m}$

vibrations occur in place of some of the $\nu_{\text{C}_m\text{C}_{\text{aryl}}}$ vibrations, are formally C–C single bond stretches due to the (approximately) orthogonal orientation of the porphyrins, and should occur in a spectral region similar to that of the $\nu_{\text{C}_m\text{C}_{\text{aryl}}}$ modes. Candidates for $\nu_{\text{C}_m\text{C}_m}$ vibrations are RR bands at 1197 (dimer), 1203 (trimer), and 1205 cm⁻¹ (tetramer), that have no analogues in the RR spectrum of the monomers. The trimer and tetramer also each exhibit another band in the 1212–1215-cm⁻¹ region that has no analogue in the RR spectrum of the monomer and is a candidate for a second $\nu_{\text{C}_m\text{C}_m}$ mode.

RR Polarization Characteristics of the meso,meso-Linked Arrays and the Monomeric Building Blocks. The polarization characteristics of the RR bands of the diaryl- and triaryl-substituted monomers and all three *meso,meso*-linked arrays are similar to one another. These RR polarization characteristics are in turn distinctly different from those of CuTPP. The RR polarization characteristics of symmetrically substituted porphyrins, such as CuTPP, are typically as follows: A_{1g} , polarized (p); A_{2g} , anomalously polarized (ap); B_{1g} and B_{2g} , depolarized (dp).²² Inspection of Table 1 reveals that the only p and ap RR bands are observed for both the diaryl- and triaryl-substituted monomers and all three *meso,meso*-linked arrays. No dp bands are observed. The depolarization ratios (ρ) of the p bands are in the range $0.3 \leq \rho \leq 0.6$; those of the ap bands are in the range $1 \leq \rho \leq 2$. The dispersion in ρ -values for individual bands does not fall outside these ranges, with one exception. The ν_{11} band of the dimer is p ($\rho \sim 0.3$) with Q-state excitation and ap ($\rho \sim 2$) with B-state excitation (Figure 5).

The polarization characteristics of the RR bands are determined by the excited-state properties of the molecules.²² The observation that the diaryl- and triaryl-substituted monomers and the *meso,meso*-linked arrays exhibit only p and ap modes is attributed to the effects of symmetry lowering in the excited state. The fact that the altered polarization occurs in the monomers indicates that the *meso* substitution pattern plays a key role in the excited-state symmetry lowering. In the case of the arrays, the symmetry lowering resulting from the different excitonic interactions along the two molecular axes may also contribute to the unusual polarization characteristics. However, the complexity of the scattering patterns precludes any accurate separation of these contributions. The ap characteristics exhibited

by modes such as $\nu_{10}(B_{1g})$ and $\nu_{11}(B_{1g})$, which are dp in CuTPP, are attributed to the A_{2g}/B_{1g} mixing that occurs because of the nature of the *meso* substitution pattern (vide supra). Likewise, it would be expected that A_{1g}/B_{2g} mixing would lead to p character for the normally dp B_{2g} modes. The only B_{2g} vibration observed is ν_{29} of the dimer at 1367 cm^{-1} , which is p, as predicted (Figure 5, Table 1).

Finally, it should be noted that the dispersion in the ρ -values observed for all of the RR bands indicates that the extent of symmetry lowering is different in the different excited states of the complexes. This is most strikingly illustrated by the behavior of the ν_{11} band of the dimer, which is ap with B-state excitation and p with Q-state excitation. The vibronic contribution to symmetry lowering, such as that which occurs in the Q(1,0) states, is also undoubtedly different along different normal coordinates. The symmetry lowering along the ν_{11} coordinate in the Q-state of the dimer is apparently sufficiently large, such that all symmetry is lost (hence, the p character of the RR band). The extent of symmetry lowering appears to be smaller along other normal modes, and ap character is retained in the RR polarization. Together, these features indicate that the vibronic character of the excited states of all of the complexes is quite complicated.

RR Enhancement Patterns of the *meso,meso*-Linked Arrays. Despite the unusual polarization characteristics observed for the RR bands of the diaryl- and triaryl-substituted monomers, the RR enhancement patterns exhibited by these monomers are similar to that of CuTPP and other more symmetrical porphyrins. In particular, for both monomers, totally symmetric modes are enhanced with B-state excitation and nontotally symmetric modes are predominantly enhanced with Q-state excitation (Figure 4). In addition, all of the totally symmetric modes enhanced with B-state excitation are derived from A_{1g} -like vibrations. Modes that become totally symmetric due to symmetry lowering are not enhanced. This general RR enhancement pattern is well understood and occurs because Franck–Condon scattering dominates with excitation into the strong B-state absorption, whereas Herzberg–Teller scattering dominates with excitation into the relatively weak Q-state absorption.²²

The RR enhancement patterns observed for the *meso,meso*-linked arrays are more complicated. As is the case for the monomers, Q-state excitation predominantly enhances nontotally symmetric modes (Figures 5–7, bottom traces). On the other hand, the RR enhancement pattern observed with B-state excitation is quite unusual and changes with the size of the array. For the dimer, $B_y(0,0)$ excitation results in a standard RR scattering pattern, wherein predominantly totally symmetric modes are enhanced (Figure 5, top trace). These totally symmetric modes are primarily derived from A_{1g} -like vibrations. Totally symmetric modes also dominate the RR spectra, with $B_x(0,0)$ excitation and at excitation energies between $B_y(0,0)$ and $B_x(0,0)$ (Figure 5, second and third traces). However, $B_x(0,0)$ excitation also elicits strong scattering from vibrations that have become totally symmetric in the low-symmetry environment, in particular $\nu_{37}(E_u)$ at 1547 cm^{-1} and $\nu_{29}(B_{2g})$ at 1367 cm^{-1} . Neither of these vibrations is typically observed with B-state excitation. Indeed, $\nu_{37}(E_u)$ is not generally RR active. The $\nu_{37}(E_u)$ and $\nu_{29}(B_{2g})$ vibrations are most likely enhanced via excited-state mixing with A_{1g} -derived vibrations. Another feature worthy of comment is the enhancement (albeit weak) of the ap ν_{11} mode at 1501 cm^{-1} , with excitation between $B_y(0,0)$ and $B_x(0,0)$ (Figure 5, second trace).

The B-state excitation RR enhancement patterns for the trimer and the tetramer are similar to one another and distinctly

different from those of the dimer. For these arrays, $B_y(0,0)$ excitation results in the expected scattering from totally symmetric modes (Figures 6 and 7, top traces). However, certain nontotally symmetric modes are also enhanced, including the ap modes ν_{11} at 1501 cm^{-1} and ν_{19} at 1531 cm^{-1} . This scattering pattern prevails with excitation between $B_x(0,0)$ and $B_y(0,0)$ (Figures 6 and 7, second traces); however, the RR enhancement of the nontotally symmetric modes is somewhat larger than those with $B_y(0,0)$ excitation. With $B_x(0,0)$ excitation, the scattering pattern changes and only totally symmetric modes are observed. However, unlike the case of the dimer, $B_x(0,0)$ excitation of the trimer and tetramer only gives rise to scattering from A_{1g} -derived vibrations. No enhancement is observed for vibrations that become totally symmetric due to symmetry lowering, in particular $\nu_{37}(E_u)$ (1547 cm^{-1}) and $\nu_{29}(B_{2g})$ (1367 cm^{-1}). Indeed, the $B_x(0,0)$ excitation RR spectra of the trimer and tetramer look like typical B(0,0) excitation spectra of symmetrical, monomeric metalloporphyrins.

A plausible explanation for the B-state RR enhancement patterns of the *meso,meso*-linked arrays is as follows: as the number of porphyrins in the array increases, the oscillator strength of the $B_x(0,0)$ absorption systematically increases. This spectral characteristic is obscured by the fact that the intensities of the $B_x(0,0)$ and $B_y(0,0)$ bands remain comparable as the array size increases. This occurs because the $B_y(0,0)$ band is a superposition of features, due to the N independent absorptions. In the case of the trimer and tetramer, the oscillator strength of the $B_x(0,0)$ transition is apparently sufficiently large, such that it effectively becomes a “super” $B_x(0,0)$ transition. Excitation into this “super” $B_x(0,0)$ transition promotes exceptionally strong Franck–Condon RR scattering. The intensity enhancement for modes derived from truly symmetric vibrations (e.g., A_{1g} modes) is apparently much larger than that for modes that only become symmetric by symmetry lowering (e.g., $\nu_{37}(E_u)$ and $\nu_{29}(B_{2g})$). Franck–Condon scattering is also strong with $B_y(0,0)$ excitation, but not as strong as with $B_x(0,0)$ excitation. In this case, the RR enhancement of A_{1g} -derived modes does not completely overpower that of modes that become totally symmetric by symmetry lowering. In addition, the energetic proximity of the single “super” $B_x(0,0)$ state and multiple “normal” $B_y(0,0)$ states affords significant vibronic coupling between these states. This vibronic coupling results in Herzberg–Teller scattering from nontotally symmetric modes with $B_y(0,0)$ excitation. This model also explains the RR scattering characteristics of the dimer. For this smaller array, the oscillator strength of the $B_x(0,0)$ transition is apparently not sufficient to move it into the “super” $B_x(0,0)$ limit. Hence, the RR enhancement of A_{1g} -derived modes does not completely overpower those of the modes that become totally symmetric by symmetry lowering. The lower oscillator strength of the $B_x(0,0)$ band of the dimer (relative to that of the trimer or tetramer) also decreases the magnitude of the Herzberg–Teller coupling between the $B_x(0,0)$ state and the $B_y(0,0)$ states. Accordingly, the RR intensity enhancement of nontotally symmetric vibrations is relatively weak, with $B_y(0,0)$ excitation.

Summary and Conclusions

The electronic and vibrational characteristics of the *meso,meso*-linked arrays are unusual from a number of respects. The B-excited states experience extremely strong uniaxial excitonic interactions. These interactions break the degeneracy of the B-excited state and give rise to a “super” $B_x(0,0)$ transition and a series of isoenergetic “normal” $B_y(0,0)$ transitions. The RR spectra of the arrays are characterized by features including (1)

the appearance of only p and ap modes in the RR spectrum, (2) the intensity enhancement of ap vibrations with B-state excitation, and (3) the large differential enhancement of symmetric versus nontotally symmetric vibrations with excitation across the B-state absorptions. All of these scattering characteristics are due to the effects of symmetry lowering. Characteristic 1 is predominantly due to symmetry lowering that results from the unsymmetrical *meso* substitution pattern. This symmetry lowering is manifested in both the ground and excited electronic states of the arrays (and monomeric building blocks). Characteristics 2 and 3 are due to the strong excitonic interactions that occur along the direction of the *meso,meso*-linkage(s) in the arrays. The strong excitonic interactions promote novel Franck–Condon and vibronic scattering mechanisms in the B state(s) of the arrays. Collectively, the studies of the *meso,meso*-linked arrays provide insight into the type of RR scattering that might be anticipated for other types of systems that exhibit strong excitonic interactions among the constituents.

Acknowledgment. This work was supported by grants from the National Institutes of Health (GM 36243 to D.F.B.), by Grant-in-Aids for Scientific Research from the Ministry of Education, Science, Sports and Culture of Japan (A.O.), and by CREST (Core Research for Evolutional Science and Technology) of Japan Science and Technology Corporation (JST) (A.O.). N.Y. thanks JSPS for a Research Fellowship for Young Scientists.

References and Notes

- (1) (a) Larkum, A. W. D.; Barret, J. *Adv. Bot. Res.* **1983**, *10*, 1. (b) Deisenhofer, J.; Epp, O.; Miki, K.; Huber, R.; Michel, H. *J. Mol. Biol.* **1984**, *180*, 385–398. (c) Hunter, C. N.; van Grondelle, R.; Olsen, J. D. *Trends Biochem. Sci.* **1989**, *14*, 72. (d) Kühlbrandt, W.; Da Neng, W.; Fujiyoshi, Y. *Nature* **1994**, *367*, 614–621. (e) McDermott, G.; Princes, S. M.; Freer, A. A.; Haworththwaite-Lawless, A. M.; Papiz, M. Z.; Cogdell, R. J.; Isaacs, N. W. *Nature* **1995**, *374*, 517–521.
- (2) Burrell, A. K.; Officer, D. L. *Synlett* **1998**, 1297–1307.
- (3) Kuciauskas, D.; Liddell, P. A.; Johnson, T. E.; Weghorn, S. J.; Lindsey, J. S.; Moore, A. L.; Moore, T. A.; Gust, D. *J. Am. Chem. Soc.* **1999**, *121*, 8604–8614.
- (4) Mak, C. C.; Bampos, N.; Sanders, J. K. M. *Angew. Chem., Int. Ed. Engl.* **1998**, *37*, 3020–3023.
- (5) Nakano, A.; Osuka, A.; Yamazaki, I.; Yamazaki, T.; Nishimura, Y. *Angew. Chem., Int. Ed. Engl.* **1998**, *37*, 3023–3027.
- (6) Drain, C. M.; Nifiatis, F.; Vasenko, A.; Batteas, J. D. *Angew. Chem., Int. Ed. Engl.* **1998**, *37*, 2344–2347.
- (7) (a) Prathapan, S.; Johnson, T. E.; Lindsey, J. S. *J. Am. Chem. Soc.* **1993**, *115*, 7519–7520. (b) Li, F.; Gentemann, S.; Kalsbeck, W. A.; Seth, J.; Lindsey, J. S.; Holten, D.; Bocian, D. F. *J. Mater. Chem.* **1997**, *7*, 1245–1262. (c) Seth, J.; Palaniappan, V.; Johnson, T. E.; Prathapan, S.; Lindsey, J. S.; Bocian, D. F. *J. Am. Chem. Soc.* **1994**, *116*, 10578.
- (8) (a) Li, F.; Diers, J. R.; Seth, J.; Yank, S. I.; Bocian, D. F.; Holten, D.; Lindsey, J. S. *J. Org. Chem.* **1999**, *64*, 9090–9100. (b) Li, J. Z.; Lindsey, J. S. *J. Org. Chem.* **1999**, *64*, 9101–9108.
- (9) Mongin, O.; Papamichael, C.; Hoyler, N.; Gossauer, A. *J. Org. Chem.* **1998**, *63*, 5568–5580.
- (10) Wennerstrom, O.; Ericsson, H.; Raston, I.; Svensson, S.; Pimlott, W. *Tetrahedron Lett.* **1989**, *30*, 1129–1132.
- (11) Osuka, A.; Liu, B.-L.; Maruyama, K. *Chem. Lett.* **1993**, 949–952.
- (12) Officer, D. L.; Burrell, A. K.; Reid, D. C. W. *Chem. Commun.* **1996**, 1657–1658.
- (13) Norsten, T.; Branda, N. *Chem. Commun.* **1998**, 1257–1258.
- (14) Osuka, A.; Tanabe, N.; Nakajima, S.; Maruyama, K. *J. Chem. Soc., Perkin Trans. 2* **1996**, 199–203.
- (15) Ichihara, K.; Naruta, Y. *Chem. Lett.* **1995**, 631–632.
- (16) Anderson, S.; Anderson, H. L.; Sanders, J. K. M. *Acc. Chem. Res.* **1993**, *26*, 469–475.
- (17) Li, J.; Arounagui, A.; Yang, S.-Y.; Diers, J. R.; Seth, J.; Kim, D.; Bocian, D. F.; Holten, D.; Lindsey, J. S. *J. Am. Chem. Soc.* **1999**, *121*, 8927–8940.
- (18) Jiang, B.; Yang, S.-W.; Jones, W. E., Jr. *Chem. Mater.* **1997**, *9*, 2031–2034.
- (19) Jiang, B.; Yang, S.-W.; Niver, R.; Jones, W. E., Jr. *Synth. Met.* **1998**, *94*, 205–210.
- (20) Jiang, B.; Yang, S.-W.; Barbini, D. C.; Jones, W. E., Jr. *Chem. Commun.* **1998**, 213–214.
- (21) Osuka, A.; Shimidzu, H. *Angew. Chem., Int. Ed. Engl.* **1997**, *36*, 135–137.
- (22) For reviews, see: (a) Procyk, A. D.; Bocian, D. F. *Annu. Rev. Phys. Chem.* **1992**, *43*, 465–496. (b) Spiro, T. G.; Czernuszewicz, R. S. *Coord. Chem. Rev.* **1990**, *100*, 541–571. (c) Spiro, T. G.; Li, X.-Y. In *Biological Applications of Raman Spectroscopy*; Spiro, T. G., Ed.; Wiley: New York, 1988; Vol. 3, pp 1–38. (d) Kitagawa, T.; Ozaki, Y. *Struct. Bonding* **1987**, *64*, 71–114.
- (23) Adar, F.; Srivastava, T. S. *Proc. Natl. Acad. Sci. U.S.A.* **1975**, *72*, 4419–4424.
- (24) Burke, J. M.; Kincaid, J. R.; Spiro, T. G. *J. Am. Chem. Soc.* **1978**, *100*, 6077–6083.
- (25) (a) Schick, G. A.; Bocian, D. F. *J. Am. Chem. Soc.* **1980**, *102*, 7982–7984. (b) Schick, G. A.; Bocian, D. F. *J. Am. Chem. Soc.* **1983**, *105*, 1830–1838.
- (26) Hofmann, J. A., Jr.; Bocian, D. F. *Inorg. Chem.* **1984**, *23*, 1177–1180.
- (27) Hofmann, J. A., Jr.; Bocian, D. F. *J. Phys. Chem.* **1984**, *88*, 1472–1479.
- (28) Boldt, N. J.; Bocian, D. F. *J. Phys. Chem.* **1988**, *92*, 581–586.
- (29) (a) Donohoe, R. J.; Duchowski, J. K.; Bocian, D. F. *J. Am. Chem. Soc.* **1988**, *110*, 6119–6124. (b) Duchowski, J. K.; Bocian, D. F. *J. Am. Chem. Soc.* **1990**, *112*, 3312–3318. (c) Duchowski, J. K.; Bocian, D. F. *Inorg. Chem.* **1990**, *29*, 4158–4160.
- (30) Tait, C. D.; Garner, J. M.; Collman, J. P.; Sattleberger, A. P.; Woodruff, W. H. *J. Am. Chem. Soc.* **1989**, *111*, 9072–9077.
- (31) Duchowski, J. K.; Bocian, D. F. *J. Am. Chem. Soc.* **1990**, *112*, 8807–8811.
- (32) Wagner, R. W.; Seth, J.; Yang, S. I.; Kim, D.; Bocian, D. F.; Holten, D.; Lindsey, J. S. *J. Org. Chem.* **1998**, *63*, 5042–5049.
- (33) Seth, J.; Palaniappan, V.; Wagner, R. W.; Johnson, T. E.; Lindsey, J. S.; Bocian, D. F. *J. Am. Chem. Soc.* **1996**, *118*, 11194–11207.
- (34) Fuhrhop, J.-H. In *Porphyryns and Metalloporphyryns*; Smith, K. M., Ed.; Elsevier: Amsterdam, 1975; pp 757–869.
- (35) Goutman, M. In *The Porphyryns*; Dolphin, D., Ed.; Academic Press: New York, 1978; Vol. 3, pp 1–165.
- (36) (a) Kasha, M.; Rawls, H. R.; El-Bakyoumi, M. A. *Pure Appl. Chem.* **1965**, *11*, 371–392. (b) Kasha, M. *Radiat. Res.* **1963**, *20*, 55–71.
- (37) Anderson, H. L. *Inorg. Chem.* **1994**, *33*, 972–981.
- (38) The exact value of ΔE is not known because the transition to the highest energy excitonic state is forbidden. Therefore, ΔE was taken to be twice the value of the difference in energy between the $B_X(0,0)$ and $B_Y(0,0)$ features. We also note that, in ref 21, the slope of the ΔE versus $2 \cos[\pi/(N+1)]$ line is given as 2100 cm^{-1} rather than the actual value of 4200 cm^{-1} . Nevertheless, the exciton coupling energy ($\sim 2100 \text{ cm}^{-1}$) is specified correctly in ref 21.
- (39) Atamian, M.; Donohoe, R. J.; Lindsey, J. S.; Bocian, D. F. *J. Phys. Chem.* **1989**, *93*, 2236–2243.
- (40) Li, X.-Y.; Czernuszewicz, R. S.; Kincaid, J. R.; Su, O.; Spiro, T. G. *J. Phys. Chem.* **1990**, *94*, 31–47.
- (41) Hu, S.; Spiro, T. G. *J. Am. Chem. Soc.* **1993**, *113*, 12029–12034.